Primary cilia are specialized calcium signaling organelles

Published as: *Nature*. 2013 December 12; 504(7479): 311–314.

Primary cilia are specialized calcium signaling organelles

Markus Delling[*,1], **Paul G. DeCaen**[*,1], **Julia F. Doerner**[1], **Sebastien Febvay**[1], and **David E. Clapham**[1,2,†]

[1]Howard Hughes Medical Institute, Department of Cardiology, Boston Children's Hospital, 320 Longwood Avenue, Boston, MA 02115, USA

[2]Department of Neurobiology, Harvard Medical School, Boston, MA 02115, USA

Summary

Primary cilia are solitary nonmotile extensions of the centriole found on nearly all nucleated eukaryotic cells between cell divisions. Only ~200-300 nm in diameter and a few microns long, they are separated from the cytoplasm by the ciliary neck and basal body. Often called sensory cilia, they are hypothesized to receive chemical and mechanical stimuli and initiate specific cellular signal transduction pathways. When activated by a ligand, Hedgehog (Hh) pathway proteins, such as Gli2 and Smoothened (Smo), translocate from the cell into the cilium[1,2]. Mutations in primary ciliary proteins are associated with severe developmental defects[3]. The ionic conditions, permeability of the primary cilia membrane, and effectiveness of the diffusion barriers between the cilia and cell body are unknown. Here we show that cilia are a unique calcium compartment regulated by a heteromeric TRP channel, PKD1-L1/PKD2-L1. In contrast to the hypothesis that polycystin (PKD) channels initiate changes in ciliary calcium that are conducted into the cytoplasm[4], we show that changes in ciliary calcium concentration ($[Ca^{2+}]_{cilia}$) occur without substantially altering global cytoplasmic calcium ($[Ca^{2+}]_{cyto}$). PKD1-L1/PKD2-L1 acts as a ciliary calcium channel controlling $[Ca^{2+}]_{cilia}$ and thereby modifying Smo-activated Gli2 translocation and Gli1 expression.

We generated a transgenic Arl13B-EGFP mouse (*Arl13B-EGFP*^{tg}) in which primary and motile cilia show spectacular fluorescence labeling throughout the animal, developed a ratiometric Ca^{2+} sensor directed specifically to cilia, and patch-clamped individual cilia and measured the resting membrane potential and a calcium-permeant conductance (I_{cilia}; see[5]). The *Arl13B-EGFP*^{tg} mice display ubiquitous green fluorescence only in primary and motile cilia but not in microvilli (Fig. 1, Extended Data Fig. 1a-c, Supplementary Video 2), 3D

---

†Correspondence and requests for materials should be addressed to D.E.C. (dclapham@enders.tch.harvard.edu).
*These authors contributed equally to this work

Online Content Any additional Methods, Extended Data display items and Source Data are available in the online version of the paper; references unique to these sections appear only in the online paper.

Author Contributions. All authors designed or conducted experiments and wrote the manuscript.

The authors declare no competing financial interests.

imaging of Arl13B-GFP reveals its exclusive localization to cilia. Staining of *wt* and *Arl13B-EGFP*^{tg} retinal pigmented cell epithelia (mRPE) cells and mouse embryonic fibroblasts (MEFs) with ciliary markers confirms that Arl13B-EGFP is indeed localized exclusively to cilia without noticeable alteration of cilia morphology (Extended Data Fig. 2).

Primary cilia are not reliably loaded with Ca^{2+}-sensitive dyes, forcing experimentalists to rely on changes in $[Ca^{2+}]_{cyto}$ as an indirect indicator of $[Ca^{2+}]_{cilia}$. To ameliorate this issue, we generated a genetically encoded calcium sensor that is targeted to the cilium by fusing GCaMP3[7] to the C-terminus of Smoothened (Smo-GCaMP3), enabling monitoring of $[Ca^{2+}]_{cilia}$ and $[Ca^{2+}]_{cyto}$ simultaneously. As shown in Extended Data Fig. 3 and Supplementary Video 3, addition of the Ca^{2+} ionophore, ionomycin, increased fluorescence in both the cytoplasm and cilium of hRPE1 cells stably expressing Smo-GCaMP3, although variation in ionomycin incorporation precludes precise $[Ca^{2+}]$ comparison between the two compartments.

To quantify $[Ca^{2+}]$ we developed a ratiometric Smo-mCherry-GCaMP3 calcium sensor[8] (Fig. 2a,b). In hRPE1 cells stably expressing Smo-mCherry-GCaMP3, the cilia-targeted GCaMP3 and mCherry fluorescence colocalized with the cilia-specific marker, acetylated tubulin (Extended Data Fig. 3e-h). To determine whether $[Ca^{2+}]_{cilia}$ could be increased without affecting $[Ca^{2+}]_{cyto}$, we ruptured the cilia membrane at the tip of the cilia (circle; Extended Data Fig. 3i, j) with an intense 1-2 s laser pulse (405 nm), leading to a rapid increase in $[Ca^{2+}]_{cilia}$ from the tip that traveled to the ciliary base (Supplementary Video 4). Peak $[Ca^{2+}]$ propagated down the cilia at a rate of 4.6 ± 0.6 μm/s, yielding an apparent diffusion constant (D_{Ca}) of 5.3 $\mu m^2/s$ (similar to 5-10 $\mu m^2/s$ for D_{Ca} in stellate cell dendrites[9]).

In order to closely monitor changes in $[Ca^{2+}]_{cyto}$ at the cilia-cytoplasm junction, we loaded the calcium indicator Fluo-4 into hRPE1 cells stably expressing Smo-mCherry-GCaMP3. Ciliary membrane rupture increased $[Ca^{2+}]_{cilia}$ and was detectable at the ciliary base after a ∼40 s delay (Fig. 2c-e and Supplementary Video 5). More distant parts of the cytoplasm remain unaffected by fluctuations at the base of the cilium. Elevation of $[Ca^{2+}]_{cyto}$ after ciliary rupture occurs infrequently and with varying delay; ∼40% of the cells did not show any elevation in the cytoplasmic side of the cilia-cell junction even 60 s after $[Ca^{2+}]_{cilia}$ had saturated (Fig. 2e). Apparently the Ca^{2+}-sensor does not hinder the diffusion of Ca^{2+} from cilium to cytoplasm after rupture: in this case the cilium fills with 2 mM $[Ca^{2+}]$, which saturates the Ca^{2+}-sensor.

Next, we asked whether the protein-dense structure at the base of the cilium might act as a localized $[Ca^{2+}]$ buffer and/or impermeant physical barrier to $[Ca^{2+}]$ entry into the cytoplasm. We loaded Smo-mCherry-GCaMP3-expressing cells with the caged calcium chelator NP-EGTA-AM and uncaged $[Ca^{2+}]$ in the cytoplasm in close proximity to the ciliary base. The velocity of this Ca^{2+} wave was 16 ± 2 μm/s in the cytoplasm *and continued at* 15 ± 2 μm/s in the cilium, indicating no significant delay of $[Ca^{2+}]$ entering the cilium from the cytoplasm (Fig. 2f and Supplementary Video 6). Since the ratio of cilium/cytoplasmic volume is exceedingly small (1:30,000), the tiny ciliary Ca^{2+} rivulet is rapidly diluted in the large cytoplasmic volume. Since the number of free calcium ions at 1 μM

concentration within the ~ 0.5 fL cilioplasm is ~200 ions at an instant in time, calcium does not perturb cytoplasmic [Ca^{2+}] substantially, nor does it initiate a measurable Ca^{2+}-induced Ca^{2+} release wave in the cytoplasm. These considerations led us to ask whether resting $[Ca^{2+}]_{cilia}$ differs from resting $[Ca^{2+}]_{cyto}$.

The K_D for the ratiometric ciliary Ca^{2+} sensor *in situ* was comparable to that in solution (625 nM vs 660 nM[7]; Extended Data Fig. 4). In 2 mM $[Ca^{2+}]_e$, resting $[Ca^{2+}]_{cilia}$ was 580 nM in hRPE cells (Fig. 3b). We also calibrated the ratiometric Ca^{2+} sensor in the cytoplasm using cells that had not yet formed a cilium (Smoothened in the plasma membrane; Fig. 3a bottom), and obtained a similar calibration curve and K_D (550 nM), suggesting that the sensor reported [Ca^{2+}] similarly in cilia and cytoplasm. The average ratio for the sensor in the cytoplasm of 0.28 ± 0.02 corresponding to a resting $[Ca^{2+}]_{cyto}$ of < 110 nM, a normal resting cytoplasmic [Ca^{2+}][10] (Fig. 3c). To test this surprisingly high resting $[Ca^{2+}]_{cilia}$ using an independent measurement, we patch-clamped Smo-EGFP-labeled cilia in the whole-cell configuration and varied free $[Ca^{2+}]_{cilia}$. High $[Ca^{2+}]_{cilia}$ (≥ 400 nM; IC_{50} = 445 nM, Fig. 3d) inactivates I_{cilia}, enabling an independent calibration of $[Ca^{2+}]_{cilia}$. We then estimated the undisturbed resting $[Ca^{2+}]_{cilia}$ by comparing the current amplitude from perforated-patch measurements with the [Ca^{2+}] calibration curve. The magnitude of I_{cilia} confirmed that $[Ca^{2+}]_{cilia}$ was ~7-fold higher than resting $[Ca^{2+}]_{cyto}$ (Fig. 3c).

We next determined the cilia's resting membrane potential (E_{cilia}) by measuring changes in response to depolarizing concentrations of extracellular potassium ($[K^+]_e$) from hRPE1 Smo-EGFP cytoplasm and from its primary cilia. Consistently, E_{cilia} was >30 mV positive to the cytoplasm (E_{cilia} =–18 ± 1 mV; E_{cyto} = –54 ± 2 mV, respectively; Fig. 3e) and significantly less $[K^+]_e$ (70 mM *vs.* 129 mM) was required to depolarize the ciliary membrane potential to 0 mV (Fig. 3f). In summary, the cilium is a functionally distinct cell compartment with respect to ions. This calcium compartment is maintained by a favorable influx/efflux ratio: the large number of calcium-permeant channels[5] or other ion channels/ transporters can easily maintain high [Ca^{2+}] in the small volume of the cilia, despite steady diffusion of Ca^{2+} into the cytoplasm at its base. An analogy is a water tower (Ca^{2+} within the cilia) connected to a large lake (cytoplasm) by a small pipe (basal body). Because ciliary [Ca^{2+}] is high (~600 nM) compared to the cytoplasm (~100 nM) calcium flows from cilium to cytoplasm, but not cytoplasm to cilia. In addition, an ~ –30 mV gradient from cilia to cytoplasm further insures asymmetry of Ca^{2+} flux. We speculate that these factors insulate cilia from the < 1 μM Ca^{2+} fluctuations that characterize cytoplasmic Ca^{2+} signaling.

What are the consequences to cell function of ciliary ion independence from the cytoplasm? As we show in DeCaen et al.[5], I_{cilia} is mediated predominantly by the heteromeric channel, PKD1-L1 and PKD2-L1. *PKD1-L1*$^{-/-}$ mice have a ciliary phenotype[11,12], but in this study we focused on the pore-forming subunit of I_{cilia}, PKD2-L1. Although PKD2-L1 was initially proposed to be a sour taste receptor, *PKD2-L1*$^{-/-}$ mice display no sour taste deficit[13]. Thus, we tested *PKD2-L1*$^{-/-}$ mice for a potential ciliary defect. While we did not observe any major organ laterality defects, we observed intestinal malrotation in about 50% of the *PKD2-L1*$^{-/-}$ knockout animals that was not observed in *wt* mice (Fig. 4a), indicating a mild penetrance of the phenotype. Intestinal malformations are associated with Sonic hedgehog (Shh) pathway defects during early development[14,15].

Treatment of mouse embryonic fibroblasts (MEF) with the Smo agonist, SAG, directly activates the Smo receptor, leading to an upregulation of *Gli1* and *Ptch1* expression[16,17]. As *PKD2-L1* is transcribed and localizes to cilia in *wt* MEF cells (Fig. 4b, Extended Data Fig. 5), we next asked whether the Shh pathway might be affected in *PKD2-L1*$^{-/-}$ mice by measuring the upregulation of Gli1 in response to stimulation with SAG. As shown in Fig. 4c,d, Gli1 protein increased from 1.9 ± 0.3 to 9.3 ± 0.7 in *wt* MEF cells stimulated for 24 h with 400 nM SAG. In contrast, SAG upregulated Gli1 from 0.9 ± 0.04 to only 3.9 ± 0.6 in *PKD2-L1*$^{-/-}$ embryonic MEF cells. As shown in Fig 4d, key members of the Shh pathway were not altered. However, *Arl13B-EGFP*^{tg} MEFs accumulate significant amounts of Gli2 at the distal tip of the cilium (Fig. 4e,f), as is required for activation of Gli2 and full activation of downstream transcription events[18]. In *PKD2-L1*$^{-/-}$ × *Arl13B-EGFP*^{tg} mutant cells, Gli2 accumulation at the ciliary tip was reduced by ∼50% compared to *wt* cells. PKD2-L1 is not required for cilia formation as ciliary length and the percentage of ciliated cells did not differ significantly between genotypes (Fig. 4g,h). Finally, we asked whether SAG stimulation itself regulates I_{cilia} and thus ciliary $[Ca^{2+}]$. Although there was no immediate effect on ciliary current stimulation with SAG, after 24 h I_{cilia} amplitude and resting $[Ca^{2+}]_{cilia}$ increased in the cilium of *wt* MEFs (Extended Data Fig. 6). This data suggests that SAG initiates recruitment of PKD2-L1 channels into the cilium rather than activating the channel.

Our results suggest that primary cilia are functionally distinct from the cytoplasm. I_{cilia} is encoded by a heteromeric PKD1-L1/PKD2-L1 channel and resting $[Ca^{2+}]_{cilia}$ is at least 0.4 μM higher than resting $[Ca^{2+}]_{cyto}$, which regulates trafficking of Hh-mediated transcription factors in the cilium. PKD2-L1 is increased by Shh pathway stimulation, most likely by channel recruitment to the cilium. Interestingly, the IFT25/IFT27 complex seems to be specific for transporting Shh components and an IFT25 mutant MEF showed an impaired Gli2 ciliary trafficking phenotype[17] similar to *PKD2-L1* mutant MEFs. Since IFT25 has a unique Ca^{2+} binding site[19], the observed Shh defect of *PKD2-L1* nulls implies that PKD2-L1 may 'tune' $[Ca^{2+}]_{cilium}$ to optimize IFT25 function. $[Ca^{2+}]_{cilium}$ is likely also adjusted by other PKD members or even other as yet unidentified ion pumps or transporters in the cilium during development, which may explain the mild phenotype of the PKD2-L1 mutant mouse compared to other Shh-deficient mutant mice (*IFT25*$^{-/-}$ and *Shh*$^{-/-}$ mice[15,17]). An alternative, but not mutually exclusive, hypothesis is that acute I_{cilia} regulation by G protein-coupled receptors and growth factors dynamically regulate ciliary trafficking. Further studies are necessary to determine whether other intermediates in the Shh pathway, such as SUFU-Gli dissociation or Gli proteolytic processing, are $[Ca^{2+}]$-dependent. A second conclusion from this work is that the cilium funnels a small but steady Ca^{2+} load into the peri-ciliary cytoplasm.

Methods Summary

A ratiometric GCAMP3-based calcium sensor was expressed in cilia to measure ciliary calcium in hRPE1 cells. A transgenic mouse model expressing GFP in cilia was generated to measure ciliary calcium and membrane potential by patch clamp recordings of cilia. Defects in Shh signaling of MEF isolated from *PKD2-L1*$^{-/-}$ mutant mice were quantified by Western blotting and ciliary localization of Gli1 protein.

Online Methods

Molecular biology

The *hArl13B* clone was obtained from Open Biosystems and cloned into the pEGFP-N1 vector. *Smo-EGFP*, *GECO1.2* and *GCaMP3* were obtained from Addgene. *GECO1.2* is an improved version of GCaMP3[20]. *GCaMP3* was spliced in frame to the 3′ end of *Smo*. The ratiometric sensor *Smo-mCherry-GCaMP3* was obtained by adding short glycine-serine linkers to the 5′ and 3′ ends of *mCherry* by PCR amplification. *mCherry* was cloned nondirectionally into *mSmo-GCaMP3* after linearization with *AgeI*. Correct orientation of *mCherry* was confirmed by sequencing. The same approach was used to add *mCherry-GECO1.2* to *hArl13B*.

Transgenic and PKD2-L1 knockout animals

We injected both a human *Arl13B-EGFP* cDNA construct and a *hArl13B-mCherry-GECO1.2* cDNA construct under the control of a chicken actin promoter (*CAG*) into the pronucleus of mouse C57/B6 oocytes and obtained 2 independent founder lines for Arl13B-EGFP and 4 independent founder lines for Arl13B-mCherry-GECO1.2. Transgenic males and females were viable and fertile. The *ScaI/HindIII* linearized plasmid was gel-purified and injected into the pronucleus of C57/BL6 oocytes at the transgenic animal core facility at Boston Children's Hospital. Oviducts of *Arl13B-EGFP*^{tg} mice were isolated as described previously[21]. All animal protocols in this work were approved by the IUACUC of Boston Children's Hospital. *PKD2-L1* knockout animals were obtained from Jackson laboratories and have been described previously[22]. P21 *PKD2L1*$^{-/-}$ and age matched *C57bl/6 wt* mice were used for morphological analysis.

Isolation of primary mouse embryonic fibroblasts (MEFs) and primary mouse retinal pigmented epithelial cells (mRPE) cells

MEFs were isolated from E15 wt, *Arl13B-EGFP*^{tg}, *Arl13B-mCherry-GECO1.2*^{tg} or *PKD2-L1*$^{-/-}$, or *PKD2-L1*$^{-/-}$ × *Arl13B-EGFP*^{tg} embryos. Freshly harvested embryos were placed in a 10 cm cell culture dish in sterile PBS. The head and inner organs were removed and used for genotyping. The body was minced in 1 ml of 0.5% trypsin (Life Technologies) with a razor blade and incubated at 37°C for 30 min. Tissue was triturated by pipetting 10-20× and the trypsin reaction was quenched by addition of 10 ml complete medium with serum (DME w/ 10% FCS). The suspension was passed through a cell strainer and plated. MEFs were seeded onto coverslips at 50% cell density and serum-starved the next day for 24 h in DMEM + 0.2% FCS for electrophysiological recordings, immunostaining, biochemistry and Gli2 translocation assays. MEF cells were not used beyond passage 4. mRPE cells were isolated as described previously[23].

Antibodies

Rabbit anti-adenylyl cyclase III, Santa Cruz; mouse anti-acetylated tubulin, Sigma-Aldrich; rabbit monoclonal anti-villin antibody, Abcam; mouse HMB45 and rabbit PKD2-L1, Thermo Scientific. Goat anti-Smoothened and anti-Gli2 antibody was a gift from A. Salic,

Harvard Medical School; Mouse monoclonal anti γ-tubulin clone GTU 88, Sigma-Aldrich; rabbit anti Gli2, Sigma Aldrich; rabbit anti-Gli1 V812, Cell Signaling.

Immunocytochemistry and confocal microscopy

Cells were fixed with 4% formaldehyde, permeabilized with 0.2% Triton X-100, and blocked by 10% goat serum in PBS. Cells were labeled with the indicated antibody and secondary goat anti-rabbit or anti-mouse fluorescently labeled IgG (Life Technologies) and Hoechst 33342 (Life Technologies). Confocal images were obtained using an Olympus FV1000 with a 60× water immersion, 1.2 N.A. objective. Images were further processed using ImageJ (NIH). Differential interference contrast images (DIC) are shown to outline cells.

3D reconstruction of cilia

E14.5 embryos were fixed in 4% PFA for 48 h and dissected. Tissue was treated with *Scale* solutions as described[24]. In brief, samples were incubated in *ScaleA2* and *ScaleB4* until they appeared transparent (3 weeks-3 months). Samples were mounted in 2% agarose in *ScaleA2* on a Petri dish. Samples were imaged in ScaleA2 with an XLUMPLFL 25× water 1.05 N.A. MPE objective. Tiles of stacks were acquired with an Olympus FV1000 MPE Exclusive with SpectraPhysics MaiTai DeepSee laser set at 915 nm. Images were acquired with single excitation in GFP and RFP channels. Subtraction eliminated autofluorescence. Tiles were stitched together using an ImageJ plug-in[25]. 3D reconstruction was done using Imaris software (Bitplane AG, Switzerland).

Cell culture and generation of stable cell lines

hRPE1 cells were transfected using TransIT-LT1 (Mirus Bio). Smo-EGFP expressing hRPE1 cells have been described previously[26]. Stable lines were selected in DMEM/F12 (Life Technologies) containing G418 (400 μg/mL) added 24 h after transfection. Stable cell lines expressing the protein were enriched by fluorescence-activated cell sorting (FACS) 2-4 weeks after initial selection. For SAG (Calbiochem) stimulation experiments, MEFs were serum-starved at 80% confluency in 3.5 cm dishes or on 12 mm coverslips for 24 h in DMEM/0.2% FCS. MEF cells were stimulated and protein levels were analysed as described[27]. In brief, MEFs were stimulated with 400 nm SAG for 24 h at 37°C. Cells were washed ×1 with PBS and lysed directly in 2× sample buffer (Life Technologies). Western blots were developed using chemiluminescence (Super Signal West Dura, Pierce Thermo) and a LAS-3000 imaging system (Fujifilm). Detection of RNA levels was performed as described previously[22].

Immunohistochemistry

15 μm formalin-fixed frozen tissue sections were permeabilized with 0.5% TX100 / PBS pH 7.4 for 15 min. Sections were blocked with 5% goat serum, 1% BSA, 0.1% fish gelatin, 0.1% TX-100 and 0.05% Tween20. For primary mouse antibodies, endogenous mouse IgGs were blocked by incubating sections with the unconjugated Fab fragment goat anti-mouse IgG for 1 h at room temperature (RT). Sections were washed twice in PBS-T and primary antibodies were diluted in blocking solution and incubated overnight at 4°C. Slides were

washed twice in PBS-T and goat anti-rabbit/anti-mouse fluorescent-labeled secondary antibodies were applied at RT for 1 h together with Hoechst 33342 nuclear dye. Sections were washed twice in PBS-T, mounted in Prolong Gold Antifade (Life Technologies) and imaged with an Olympus FV1000; water immersion 60×, 1.2 N.A. objective. Images were further processed using ImageJ (NIH).

Electrophysiology

Unless otherwise stated, all experimental conditions and methods are described in DeCaen et al[28]. For the experiments in Fig. 3d, intracellular free [Ca^{2+}] was calculated using the Maxchelator website (maxchelator.stanford.edu) and formulated by titrating $CaCl_2$ in 10 mM BAPTA-Cs buffering conditions. The resting membrane potential measurements from the cell and cilia were made in current-clamp mode. Electrical access was established in the perforated-patch configuration using Amphotericin B. Electrodes contained (in mM): 95 K-Aspartate, 30 KCl, 10 HEPES, 10 NaCl, 2 $MgCl_2$, 5 EGTA, 100 nm free Ca^{2+}. Extracellular solutions in Fig. 3e contained one of following ratios of NaCl / KCl (mM): 140/5, 135/10, 125/20, 75/70, 5/145; and 10 HEPES, 1 $MgCl_2$ and 1.8 $CaCl_2$. Intraciliary [Ca^{2+}] was equilibrated with the known pipette [Ca^{2+}] in whole-cilia recordings. Note that increasing $[Ca^{2+}]_{cilia}$ inhibits I_{cilia}. The dose-response curve was fit to the Hill equation (IC50 = 445 ± 18 nm) and used as a calibration curve. We estimated resting free $[Ca^{2+}]_{cilia}$ by comparing this curve to the current amplitude measured in perforated patches (where internal cilia calcium levels are unperturbed).

Ca^{2+} imaging in cilia

Smo-GCaMP3 and Smo-mCherry-GCaMP3 were imaged on an Olympus FV1000 at a frame interval of 250 or 64 ms. Ionomycin incorporates into both the plasma membrane and cilia; the ratios of F GCaMP3/F mCherry, reflecting changes in [Ca^{2+}], rise simultaneously in the cytoplasm and cilium. Imaging of [Ca^{2+}] transients from cilium to cytoplasm: Smo-mCherry-GCaMP3 hRPE1 cells were serum-starved for 4-5 days and loaded with Fluo4-AM at 25°C for 60 min in imaging buffer (150 mM NaCl, 2 mM $CaCl_2$, 1 mM $MgCl_2$, 10 mM glucose, 2 mM HEPES, pH 7.4) and then washed for 10–30 min. Cells with cilia extending beyond the cell body were chosen for experiments to avoid possible induction of cytoplasmic calcium signals by membrane rupture. Images were acquired as sequential scans at a frame interval of 2.20 s with spectral detectors set for GFP and mCherry emission on an Olympus FV1000 equipped with a SIM scanner. PMT and offset were adjusted for each channel such that the 16-bit pixel intensity was in the 1000 range in the GFP channel and 2500-3000 for the mCherry channel before each experiment. Under these settings GCaMP3 in the GFP channel did not reach pixel saturation after ionomycin stimulation. The ciliary membrane was ruptured using the SIM scanner coupled to a 405 nm laser. The region of interest (ROI) for photobleaching was chosen to cover the tip of the cilium; 405 nm laser intensity was set to 25% and pulse duration set to 2 s. Changes of $\Delta F/F > 10\%$ for three consecutive scans in the cytoplasm were considered significant. Cytoplasmic [Ca^{2+}] was raised by loading hRPE1 Smo-mCherry-GCaMP3 cells with o-Nitrophenyl EGTA AM (NP-EGTA AM) for 30 min at RT. Calcium was uncaged in the cytoplasm near the base of the cilium with a SIM scanner by a short (30 ms) 405 laser pulse. Diffusion of cytoplasmic Ca^{2+} to the cilium was measured by imaging changes in GCaMP3 fluorescence of Smo-mCherry-

GCaMP3 in the line-scanning mode – the line scanned the cytoplasm and the proximal side of the cilium. Apparent [Ca^{2+}] diffusion speed was 15.8 ± 1.7 μm/sec for the cytoplasm *vs.* 14.9 ± 2.1 μm/sec in the cilium, indicating no significant delay of Ca^{2+} entering the cilium from the cytoplasm. Representative traces are shown in figures. All images were analysed using ImageJ (NIH) and Origin 8 (OriginLab).

Diffusion coefficient, D_{Ca}

The 405 nm SIM laser was used to rupture the tip of a cilium and allow Ca^{2+} from the external solution (2 mM) to diffuse along the shaft towards the basal barrier. The cilium is modeled with one-dimensional diffusion assuming a constant supply at the boundary (ruptured tip), with diffusion length given by $L = 2(Dt)^{½}$. The measured fluorescence increase (GCaMP3) along the ciliary shaft immediately following tip rupture progresses at 4.6 ± 0.6 μm/s, thus providing an estimate for D_{Ca} of 5.3 $\mu m^2/s$. The volume of a cilium is roughly 0.5 fL, containing <200 free Ca^{2+} ions at 1 μM concentration. We are aware that the number of Ca^{2+} sensor proteins is thus a significant fraction of Ca^{2+} ions and will tend to 'clamp' reported levels to the K_D of the indicator. For this reason we estimated ciliary [Ca^{2+}] by an independent method that does not depend on calcium-binding proteins as calcium sensors. However, D_{Ca} is probably a low estimate since the Ca^{2+}-sensor protein may be a significant immobile buffer.

Calibration of the ratiometric Smo-mCherry-GCaMP3 sensor

Standard solutions of various [Ca^{2+}] concentrations were prepared ranging from ∼10 nm to 50 μM by adjusting the ratio of EGTA and $CaCl_2$ in each preparation to clamp free [Ca^{2+}] at the desired value. The solutions contained 137 mM NaCl, 5.4 mM KCl, 10 mM HEPES, 5 mM EGTA and $CaCl_2$ ranging from 0 to 5.04 mM (corresponding to 50 μM free [Ca^{2+}]).

For imaging, hRPE1 cells were plated onto 12 mm glass coverslips, serum-starved for 4-5 days to allow for cilia formation, and imaged in the various standard solutions following digitonin membrane permeabilisation. Briefly, coverslips were washed ×2 in Ca^{2+}-free solution to remove residual Ca^{2+} and incubated in the Ca^{2+} standard solution. The samples were then imaged using an Olympus Fluoview FV1000 laser point-scanning confocal microscope (60× water immersion, 1.2 N.A. objective) with spectral detectors set up for optimal detection of GFP and mCherry fluorescence with sequential excitation with 488 nm and 543 nm lasers, respectively. The settings were adjusted for a GCaMP3 signal in the 1000 sub-range and mCherry signal in the 2000 sub-range of the 16-bit intensity range. Identical settings were used for all Ca^{2+} standard solutions. Subsequently, the cells were permeabilized on the microscope stage by addition of an identical volume (0.5 mL) of 32 μM digitonin dissolved in the same Ca^{2+} standard, resulting in a final concentration of ∼16 μM digitonin. Images were acquired for multiple fields of view after allowing permeabilisation to occur for ∼1 min. Cytoplasmic [Ca^{2+}] was measured in RPE cells that had not formed a cilium and thus had significant levels of Smoothened-mCherry-GCaMP3 protein in the plasma membrane.

To obtain the standard calibration curve, the acquired images were processed with ImageJ in the following way. Briefly, after background subtraction, the images were thresholded in the

mCherry channel to only take into account pixels with a minimum expression level of the sensor (a threshold of 20× background signal was generally used). Dividing the GCaMP3 fluorescence image by the mCherry channel intensity generated ratio images. ROIs exclusively located in cilia of multiple cells were selected, and the average ratios measured for multiple cells and coverslips were reported. The average ratios obtained were plotted as a function of free [Ca^{2+}] and the resulting points were fitted with a sigmoid curve. Images in Figure 3a-d were acquired using the same acquisition settings as in Extended Data Figure 5.

For quantification of Gli2 at ciliary tips, MEF isolated from Arl13B EGFP^{tg} and *PKD2-L1*$^{-/-}$ × Arl13B EGFP^{tg} mice were stained with anti-Gli2 antibody[29]. Cilia were outlined in ImageJ based on the EGFP signal. Mean background signal in the Gli2 channel was determined using ImageJ, multiplied by 1.2 and subtracted from the image. Integrated fluorescence intensity was measured within the ciliary outline. Gli2 quantitation was compiled from measurements of 40 cilia from MEF each isolated from 3 *wt* and 5 *PKD2-L1*$^{-/-}$ embryos.

Data analysis—Group data are presented as mean ± SEM. Statistical comparisons were made using unpaired t tests (Origin 8). Statistical significance is denoted with asterisk (* $p < 0.05$; ** $p < 0.01$)

Extended Data

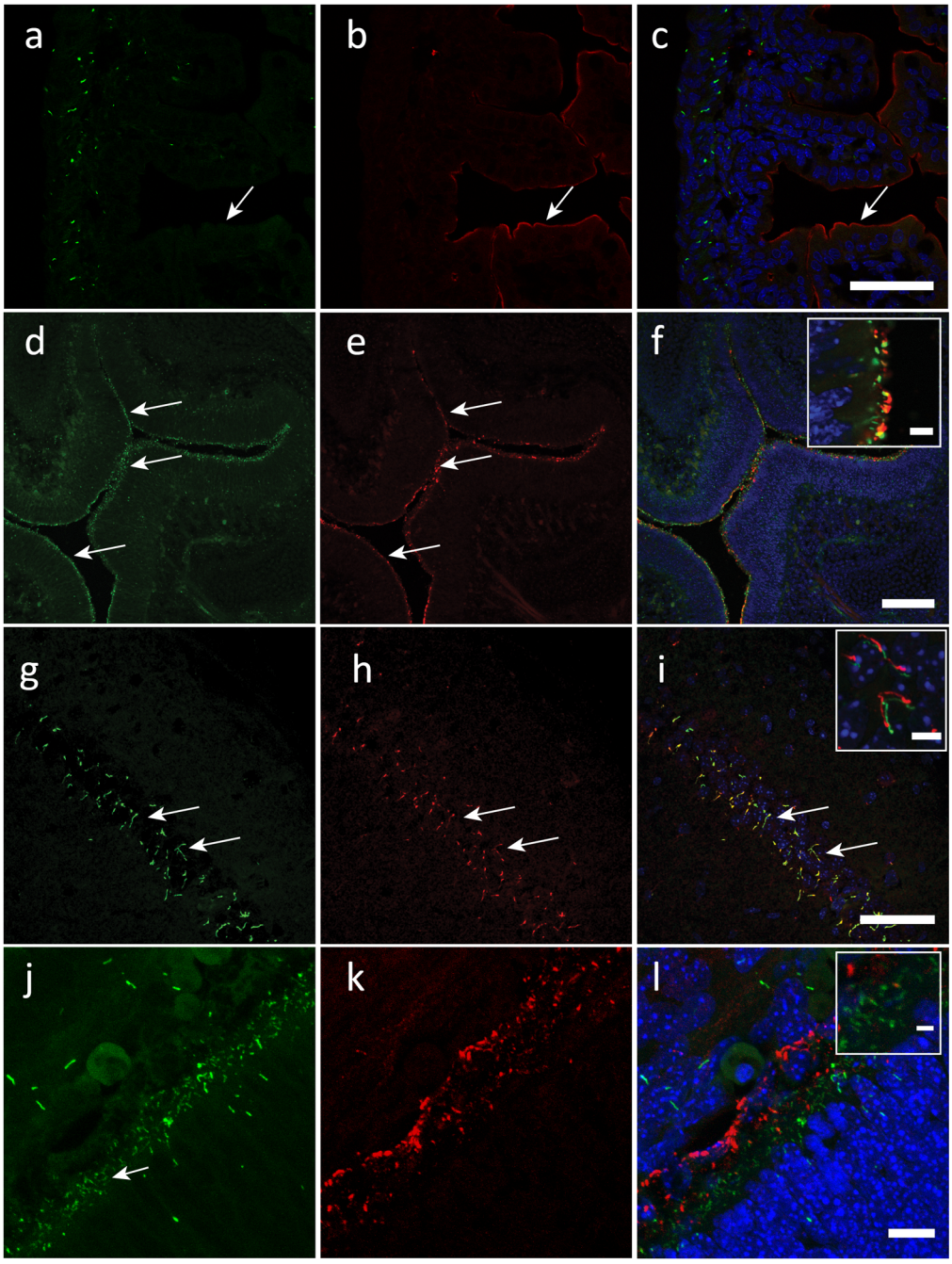

Extended Data Figure 1. Arl13B-EGFP identifies primary and motile cilia in transgenic mouse tissue

Frozen tissue sections were prepared from (**a-c**) P0 intestine; (**d-f**) E15 nasal cavity; (**g-i**) 6-week-old hippocampus; (**j-l**) P0 retina from *Arl13B-EGFP*^{tg} mice. First column, *Arl13B-EGFP*^{tg} (green) fluorescence; second column (red) labels villin in **b**, adenylyl cyclase III (ACIII) in **e**, **h**, or HMB-45 (*h*uman *m*elanoma *b*lack antibody, retinal pigmented epithelial cells) in **k**.

a-c. Intestine: EGFP fluorescence in **a** does not overlap with the anti-villin staining in **b** as shown in the merged image in **c**, indicating that Arl13B-EGFP is absent from microvilli (arrows). Scale bar, 100 μm.

d-f. Nasal cavity, (**d**) several Arl13B-EGFP-positive cilia (arrows) that face the lumen of the turbinate colocalize with ACIII (**e**) as shown in the merged image (**f**). Scale bar, 100 μm. Insert shows magnification of nasal cavity surface. Scale bar of inset in **f**, 5 μm.

g-i. CA1 region of hippocampus: (**g**) Prominent cilia (arrows) overlap with ACIII staining (**h**) as shown in the merged image (**i**). Scale bar, 50 μm. Insert shows magnification of hippocampal cilia. Inset scale bar, 5 μm. Merged red and green channels were offset for clarity (inset).

j-l. Retinal pigmented epithelia (RPE): (**j**) Short cilia (arrow) are visible at the intersection between RPE (labeled with HMB-45 antibody, (**k**) and developing photoreceptor cells, as shown in the merged image (**l**). Scale bar, 10 μm. Insert shows magnification of RPE/photoreceptor interface. Inset scale bar, 2 μm.

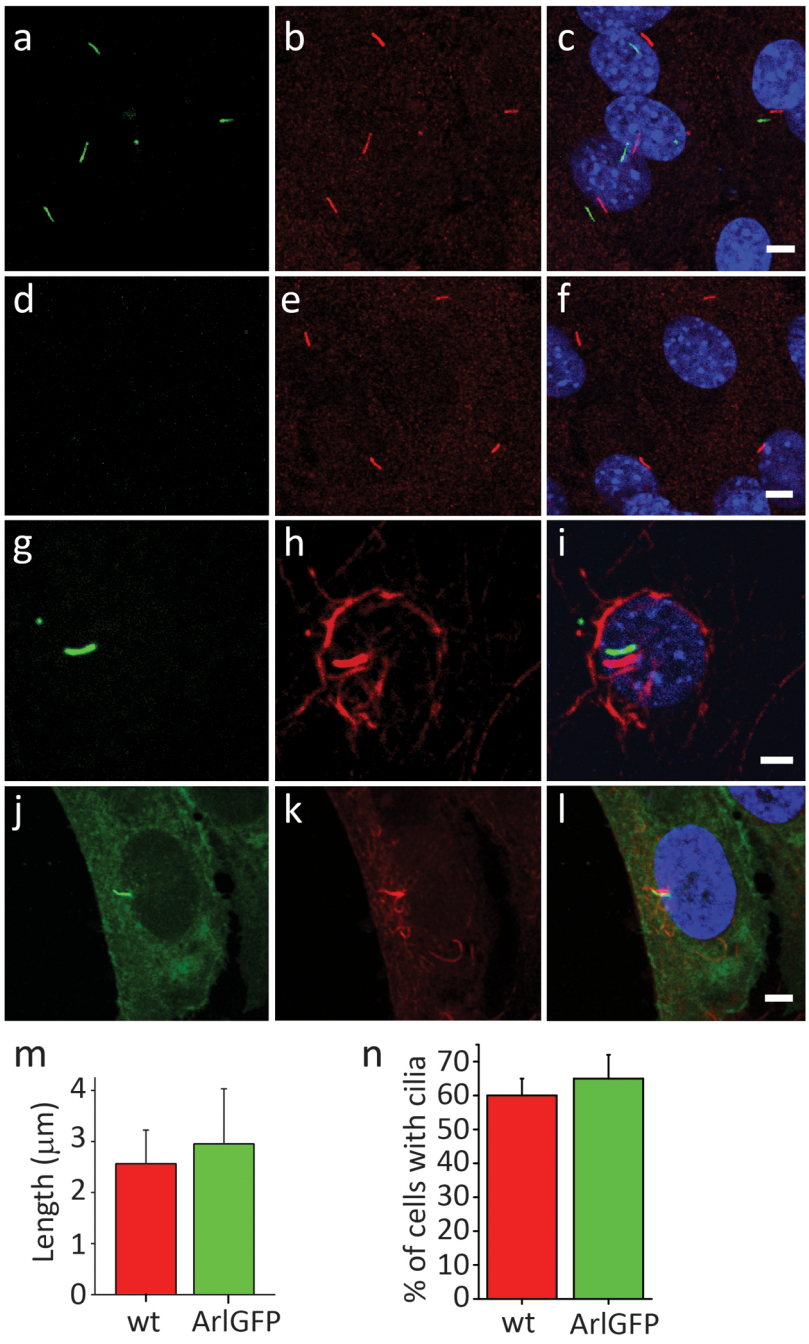

Extended Data Figure 2. Arl13B-EGFP labels a primary cilium in cultured MEF and RPE cells

First column shows *Arl13B-EGFP*^{tg} (green) fluorescence; second column labels ACIII (**b, e**) or (**h, k**) acetylated tubulin. Third column: merged red and green channels were offset for clarity.

(**a-c**) Primary mouse embryonic fibroblasts (MEF) of *Arl13B-EGFP*^{tg} and (**d-f**) *wt* mice isolated from E14.5 embryos. Arl13B-EGFP co-localizes with ciliary ACIII in **c**. MEFs isolated from *wt* mice show no fluorescence in the cilium (488 nm excitation).

(**g-i**) Primary RPE cells isolated from P12 *Arl13B-EGFP*^{tg} mice. Cells were fixed and stained with antibody to acetylated tubulin. Arl13B-EGFP (**g**) exclusively localized to the primary cilium identified by antibody to acetylated tubulin (**h, i**).

(**j-l**) Stable cell line (hRPE1) expressing Smo-EGFP. After 2 days of serum starvation, Smo-EGFP labeled the primary cilium of hRPE1 cells (**j**) as indicated by acetylated tubulin labeling (**k, l**). Scale bar in **c, f, i, l**; 5 μm.

(**m, n**) To determine whether Arl13B-EGFP expression adversely affected ciliogenesis, ciliary length and percent of cells with cilia were quantified from *wt* and Arl13B-EGFP-expressing MEFs stained by anti-acetylated tubulin. (**m**) Ciliary length was similar in *wt* and Arl13B-EGFP-expressing MEFs (2.6 ± 0.5 μm vs. 2.9 ± 0.8 μm, respectively, n=200). (**n**) The number of cells with cilia was also comparable between *wt* and Arl13B-EGFP-expressing MEFs (60.2% ± 5.1% vs. 65.5% ± 7.3%; n=120).

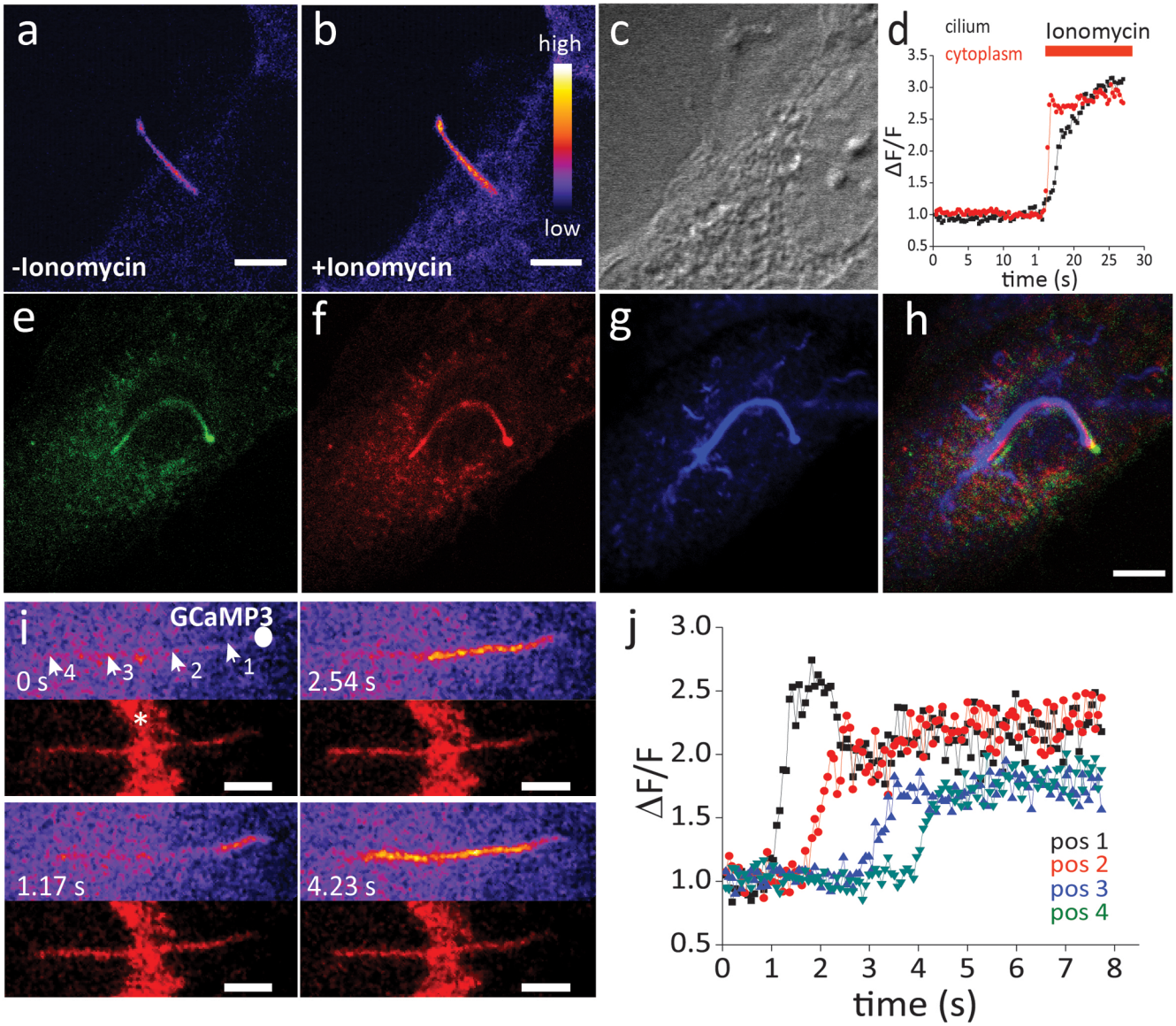

Extended Data Figure 3. Ciliary [Ca^{2+}] changes in stably-transfected RPE cell cilia

(**a-c**) Live hRPE1 cells stably expressing Smo-GCaMP3 were treated with 5 μM ionomycin. Fluorescence increases were measured in the cilium and cytoplasm. Image in (**c**) is DIC. (**d**) Changes in fluorescence (ΔF/F) of the calcium sensor, GCaMP3, are plotted for both cytoplasm and cilium. (**e-h**) hRPE1 cells expressing Smo-mCherry-GCaMP3 were stained with acetylated tubulin. GCaMP3 (**e**) and mCherry (**f**) fluorescence overlaps with acetylated tubulin staining (**g, h**). Scale bar, 5 μm; merged channels were offset for clarity. (**i**) The tip of a cilium was ruptured with an intense 1 s laser pulse (405 nm, hRPE1 cell expressing Smo-mCherry-GCaMP3). Circle indicates area of rupture. Numbered arrowheads indicate positions where changes in fluorescence were measured. Star (*****) indicates mCherry fluorescence outside of cilium, indicating that some Smo-mCherry-GCaMP3 is retained in the ER. (**j**) Quantification of changes in fluorescence at the positions marked in **i**. Rupture of the ciliary membrane rapidly increases $[Ca^{2+}]_{cilia}$ at the tip and travels along the cilium at 4.6 ± 0.6 μm/s (n=16).

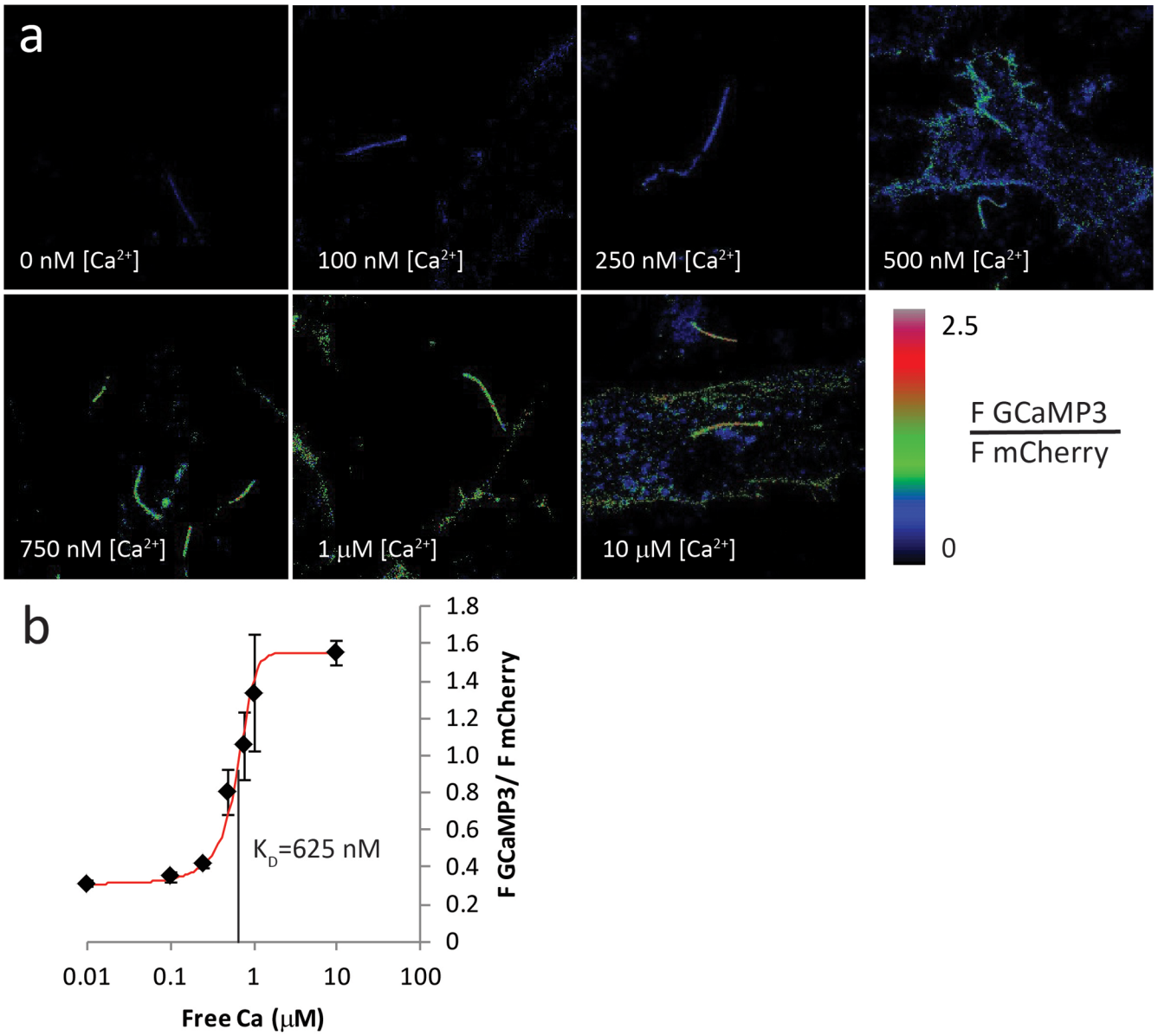

Extended Data Figure 4. $[Ca^{2+}]_{cilia}$ calibration

(**a**) Images of hRPE1 cells stably expressing Smo-mCherry-GCaMP3 were acquired after permeabilisation with 15 μM digitonin in varying extracellular $[Ca^{2+}]$. (**b**) Averages of several ratios (n = 12-16; ± S.D.) per concentration are plotted against free $[Ca^{2+}]$, yielding the calibration curve for Smo-mCherry-GCaMP3: K_D = 625 nM.

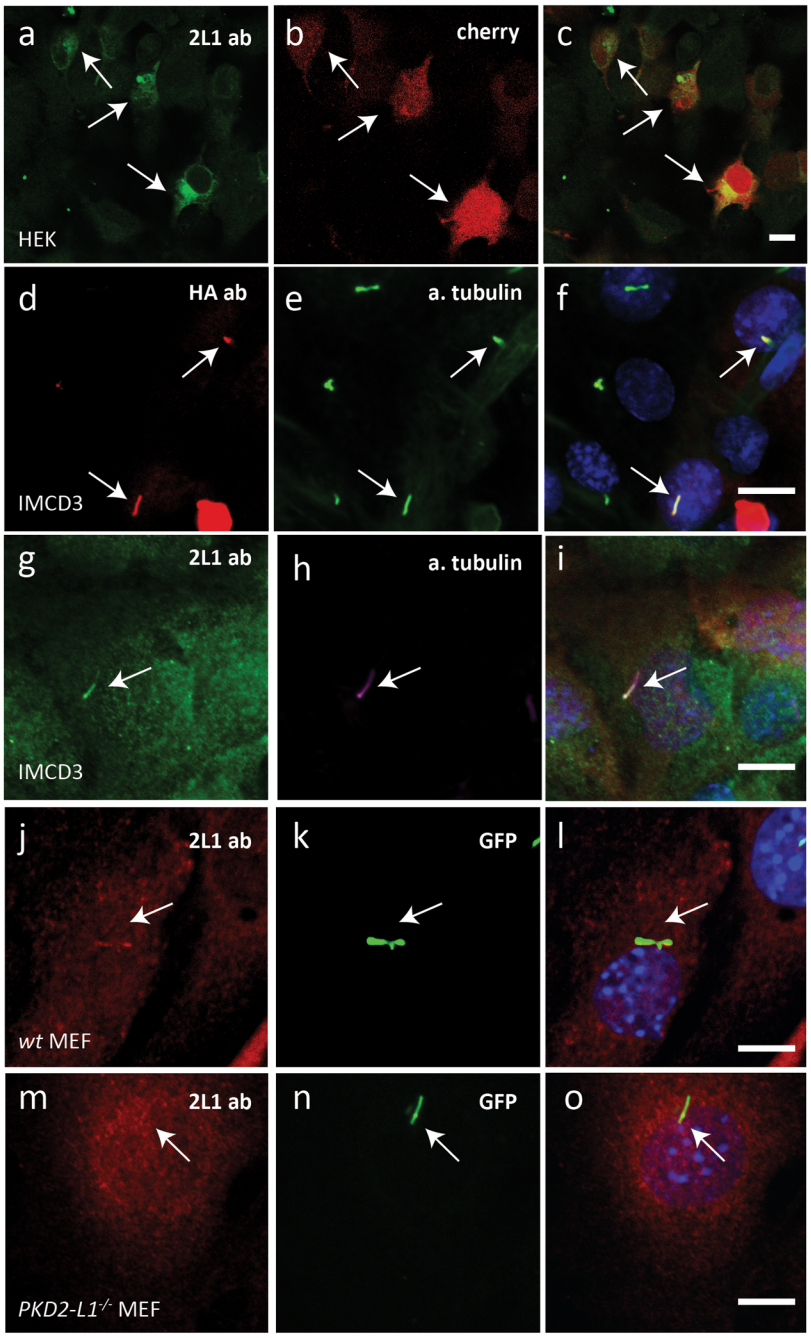

Extended Data Figure 5. Overexpressed and endogenous PKD2-L1 localizes to the primary cilium

(**a-c**) rabbit anti-PKD2-L1 (Thermo Scientific) recognizes overexpressed PKD2-L1. HEK cells were transfected with hPKD2-L1-IRES mCherry construct and stained with PKD2-L1 ab. PKD2-L1 staining (**a**) is specific to cells that also express mCherry (**b**). (**c**) overlay. (**d-f**) overexpressed hPKD2-L1 localizes to the primary cilium in mIMCD3 cells. mIMCD3 cells were transfected with HA-tagged hPKD2-L1 and stained with an anti-HA ab (**d**) and

anti acetylated tubulin ab (**e**). HA immunoreactivity is visible both in the cytoplasm and cilium. (**f**) overlay

(**g-h**) PKD2-L1 antibody labels the primary cilium of mIMCD3 cells. (**g**) Confluent mIMCD3 cells were stained with anti-PKD2-L1 ab used in **a** and (**h**) acetylated tubulin ab to label cilia. PKD2-L1 immunoreactivity is visible in the primary cilium. (**i**) overlay.

(**j-o**) Primary mouse embryonic fibroblasts (MEF) of *Arl13B-EGFP*^{tg} (**j-l**) and *Arl13B-EGFP*^{tg} × *PKD2-L1*$^{-/-}$ mice (**m-o**) isolated from E14.5 embryos were stained with anti-PKD2-L1 ab used in (**a**). In *Arl13B-EGFP*^{tg} MEF PKD2L1 immunoreactivity (**j**) colocalizes with Arl13B-EGFP signal (**k**) labeling the primary cilium. (**l**) overlay. (**m-o**) PKD2-L1 staining is absent in cilia of *Arl13B-EGFP*^{tg} × *PKD2L1*$^{-/-}$ mice. Scale bars = 10 μm.

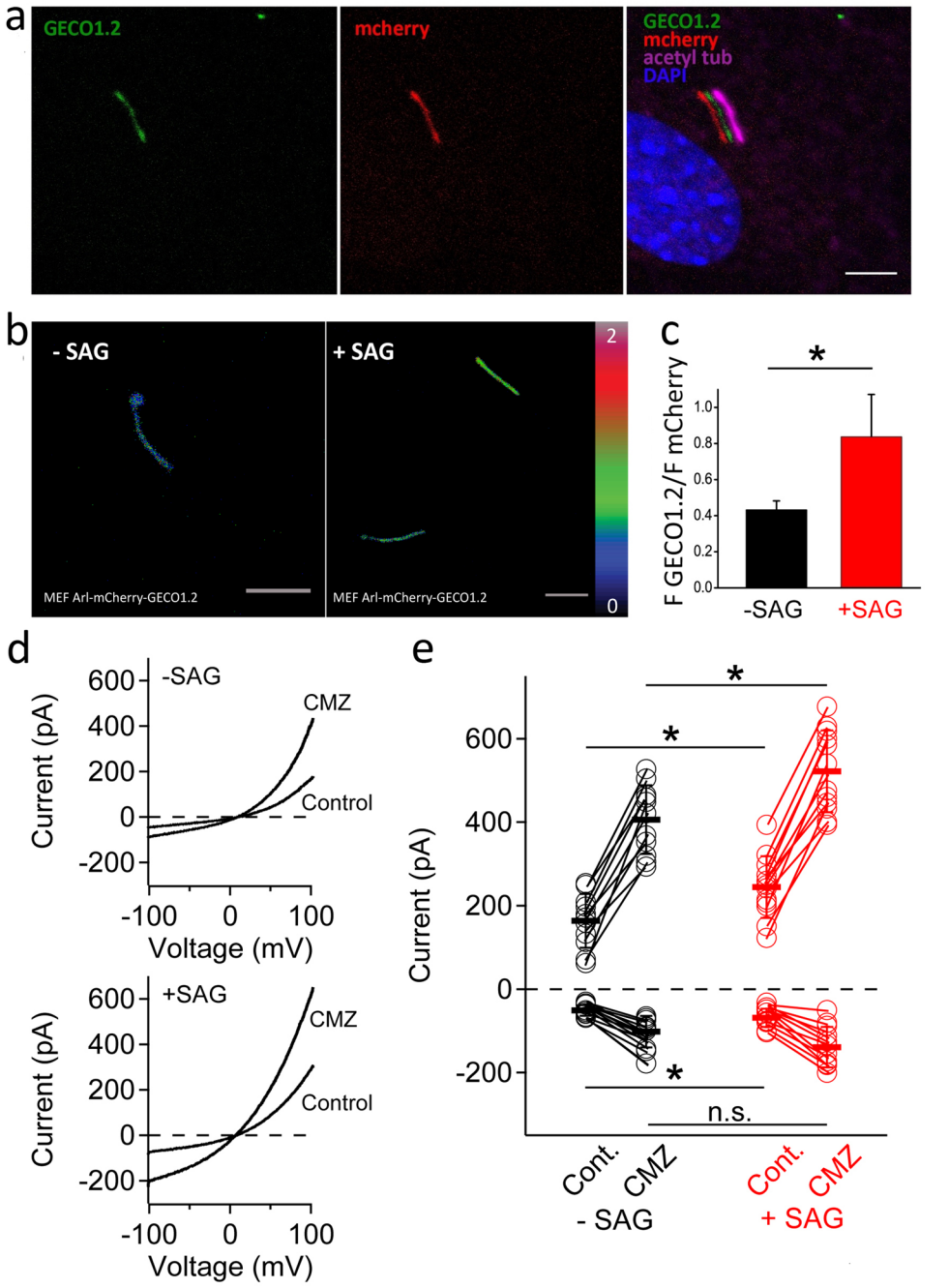

Extended Data Figure 6. $[Ca^{2+}]_{cilia}$ increases 24 h after SAG stimulation

(**a**) MEF cells expressing Arl13B-mCherry-GECO1.2 were stained with acetylated tubulin. GECO1.2 and mCherry fluorescence overlaps with acetylated tubulin staining. Scale bar, 5 μm; merged channels were offset for clarity. (**b**) Ratio maps of MEFs isolated from Arl13B-mCherry-GECO1.2 mice stimulated with 0.05% DMSO (*left*) or 400 nM SAG (*right*) for 24 h. Scale bar, 5 μm. (**c**) Quantification of ciliary GECO1.2 / mCherry ratios obtained for MEF cells with and without SAG stimulation. Ratio increases from 0.4 ± 0.05 to 0.8 ± 0.2 after SAG stimulation (*p<0.05; n=20-30 cilia). (**d**) Example ciliary current measured from

MEFs treated with 500 nM SAG (Smo agonist) or with DMSO vehicle (0.05%) in culture for 24-36 h in control conditions and after activation with 10 μM calmidazolium (CMZ). (**e**) Scatter and whisker (± S.D.) plots from cilia show total outward (+100 mV) and inward (-100 mV) current measured for both treatment groups. Averages are indicated by the thick horizontal lines and individual cilium current magnitudes are represented as circles. P-values resulting from Student's t-test comparing treatment groups are indicated (*< 0.05; n = 11 cilia).

Supplementary Material

Refer to Web version on PubMed Central for supplementary material.

Acknowledgments

We thank the Mouse Gene Manipulation Facility of the Boston Children's Hospital Intellectual and Developmental Disabilities Research Center (IDDRC; NIHP30-HD 18655). We thank the Image and Data Analysis Core (IDAC) at Harvard Medical School for help with 3D reconstruction. We also thank Adrian Salic for anti-Smo and anti-Gli2 antibodies. Paul DeCaen was supported by NIH T32-HL007572. We thank Michaela Desai for graphical assistance and Alexander von Gise and Hanna Tukachinsky (Harvard Medical School) and the members of the Clapham laboratory for advice and discussion.

References

1. Corbit KC, et al. Vertebrate Smoothened functions at the primary cilium. Nature. 437:1018–1021. [PubMed: 16136078]
2. Huangfu D, Anderson KV. Cilia and Hedgehog responsiveness in the mouse. Proc Natl Acad Sci U S A. 102:11325–11330. [PubMed: 16061793]
3. Goetz SC, Anderson KV. The primary cilium: a signalling centre during vertebrate development. Nat Rev Genet. 11:331–344. [PubMed: 20395968]
4. Praetorius HA, Spring KR. Bending the MDCK cell primary cilium increases intracellular calcium. J Membr Biol. 184:71–79. [PubMed: 11687880]
5. DeCaen PG, Delling M, Vien TN, Clapham DE. Direct recording and identification of the calcium channel of primary cilia. Nature. xxxxxx.
6. Hama H, et al. Scale: a chemical approach for fluorescence imaging and reconstruction of transparent mouse brain. Nat Neurosci. 14:1481–1488. [PubMed: 21878933]
7. Tian L, et al. Imaging neural activity in worms, flies and mice with improved GCaMP calcium indicators. Nat Methods. 6:875–881. [PubMed: 19898485]
8. Yasuda R, et al. Imaging calcium concentration dynamics in small neuronal compartments. Sci STKE. 2004:pl5. [PubMed: 14872098]
9. Soler-Llavina GJ, Sabatini BL. Synapse-specific plasticity and compartmentalized signaling in cerebellar stellate cells. Nat Neurosci. 9:798–806. [PubMed: 16680164]
10. Clapham DE. Calcium signaling. Cell. 131:1047–1058. [PubMed: 18083096]
11. Vogel P, et al. Situs inversus in Dpcd/Poll-/ -, Nme7-/ -, and Pkd1l1-/ - mice. Vet Pathol. 47:120–131. [PubMed: 20080492]
12. Field S, et al. Pkd1l1 establishes left-right asymmetry and physically interacts with Pkd2. Development. 138:1131–1142. [PubMed: 21307093]
13. Horio N, et al. Sour taste responses in mice lacking PKD channels. PLoS One. 6:e20007. [PubMed: 21625513]
14. Martin V, Shaw-Smith C. Review of genetic factors in intestinal malrotation. Pediatr Surg Int. 26:769–781. [PubMed: 20549505]
15. Ramalho-Santos M, Melton DA, McMahon AP. Hedgehog signals regulate multiple aspects of gastrointestinal development. Development. 127:2763–2772. [PubMed: 10821773]

16. Humke EW, Dorn KV, Milenkovic L, Scott MP, Rohatgi R. The output of Hedgehog signaling is controlled by the dynamic association between Suppressor of Fused and the Gli proteins. Genes Dev. 24:670–682. [PubMed: 20360384]
17. Keady BT, et al. IFT25 links the signal-dependent movement of Hedgehog components to intraflagellar transport. Dev Cell. 22:940–951. [PubMed: 22595669]
18. Kim J, Kato M, Beachy PA. Gli2 trafficking links Hedgehog-dependent activation of Smoothened in the primary cilium to transcriptional activation in the nucleus. Proc Natl Acad Sci U S A. 106:21666–21671. [PubMed: 19996169]
19. Bhogaraju S, Taschner M, Morawetz M, Basquin C, Lorentzen E. Crystal structure of the intraflagellar transport complex 25/27. EMBO J. 30:1907–1918. [PubMed: 21505417]
20. Zhao Y, et al. An expanded palette of genetically encoded Ca(2)(+) indicators. Science. 333:1888–1891. [PubMed: 21903779]
21. Miki K, Clapham DE. Rheotaxis Guides Mammalian Sperm. Curr Biol.
22. Horio N, et al. Sour taste responses in mice lacking PKD channels. PLoS One. 6:e20007. [PubMed: 21625513]
23. Gibbs D, Williams DS. Isolation and culture of primary mouse retinal pigmented epithelial cells. Adv Exp Med Biol. 533:347–352. [PubMed: 15180284]
24. Hama H, et al. Scale: a chemical approach for fluorescence imaging and reconstruction of transparent mouse brain. Nat Neurosci. 14:1481–1488. [PubMed: 21878933]
25. Preibisch S, Saalfeld S, Tomancak P. Globally optimal stitching of tiled 3D microscopic image acquisitions. Bioinformatics. 25:1463–1465. [PubMed: 19346324]
26. Kim J, et al. Functional genomic screen for modulators of ciliogenesis and cilium length. Nature. 464:1048–1051. [PubMed: 20393563]
27. Keady BT, et al. IFT25 links the signal-dependent movement of Hedgehog components to intraflagellar transport. Dev Cell. 22:940–951. [PubMed: 22595669]
28. DeCaen PG, Delling M, Vien TN, Clapham DE. Direct recording and identification of the calcium channel of primary cilia. Nature. xxxxxx.
29. Tukachinsky H, Lopez LV, Salic A. A mechanism for vertebrate Hedgehog signaling: recruitment to cilia and dissociation of SuFu-Gli protein complexes. J Cell Biol. 191:415–428. [PubMed: 20956384]

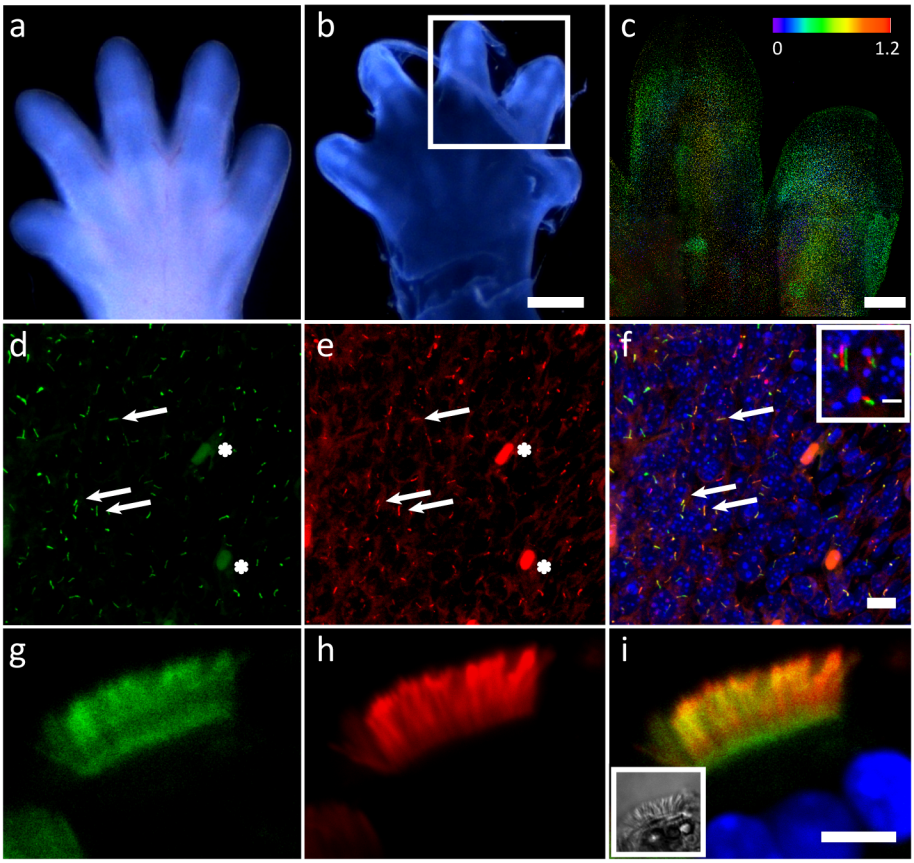

Figure 1. ArlGFP localizes to primary cilia and motile cilia *in vivo*

(**a**) Fixed paw of E14.5 embryo, and (**b**) after incubation in *ScaleA2*. Insert indicates area where z-stacks from 0 to 1.2 mm depth were acquired. Scale bar, 500 μm. (**c**) Arl13B-EGFP expression in E14.5 paw. 3 × 4 z-stacks were stitched together, depth color-coded and projected onto a plane. Scale bar, 200μm. (**d-f**) EGFP-positive cilia are present in fibroblasts within the digit (*arrows*) that overlap with ACIII labeling in **e** and merged in **f**. Scale bar = 10 μm; insert, 3 μm; asterisks indicate autofluorescence. Red and green channels are offset to visualize colocalization. (**g-i**) Motile cilia in the Fallopian tube express Arl13B-EGFP (**g**) that overlaps with acetylated tubulin (**h**). Overlay (**i**). Insert in (**i**) is DIC image. Scale bar, 5 μm.

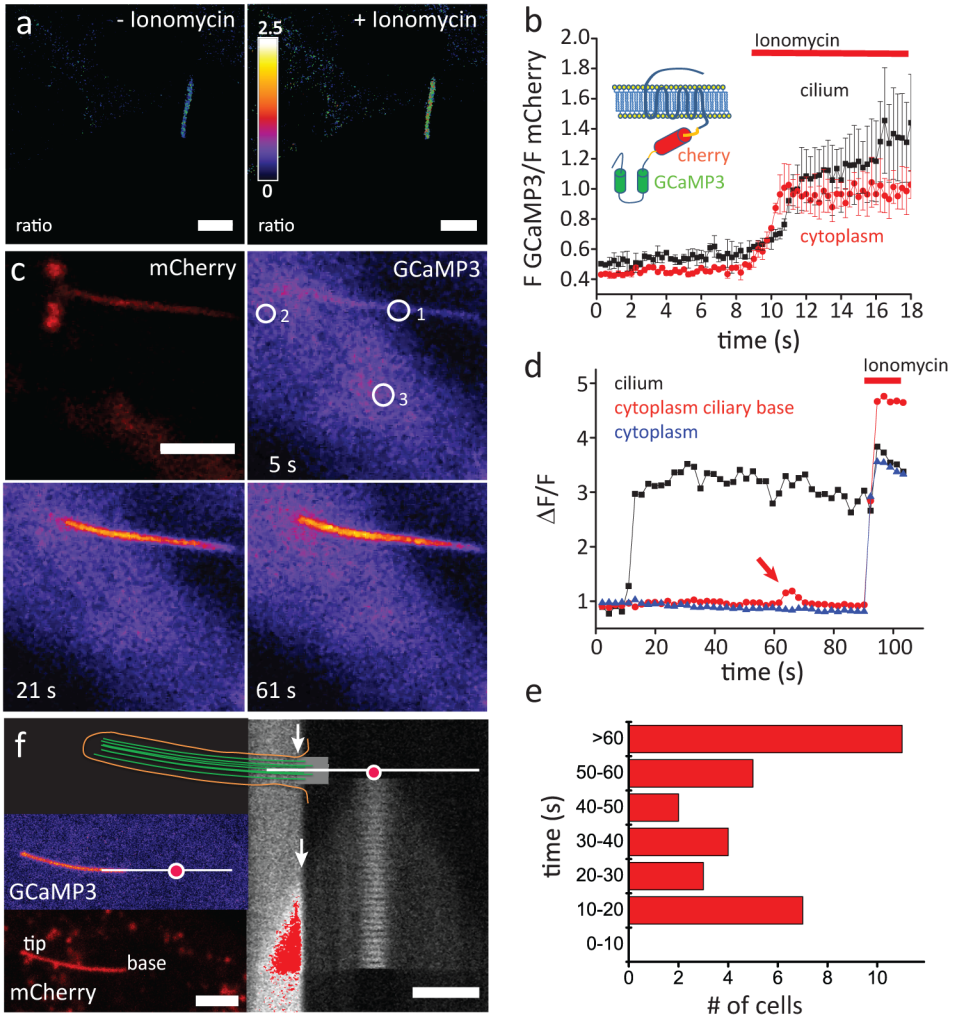

Figure 2. Smo-mCherry-GCAMP3 localizes to the primary cilium and reports ciliary $[Ca^{2+}]$. $[Ca^{2+}]_{cilia}$ is poorly coupled to $[Ca^{2+}]_{cyto}$

(a) hRPE1 cells expressing Smo-mCherry-GCaMP3 were treated with 5 μM ionomycin and changes in fluorescence were measured in the cilium and cytoplasm. (**b**) Schematic of ratiometric calcium sensor and quantified fluorescence. (**c, d**) After rupture of the ciliary tip with a laser pulse (t = 10 s), $[Ca^{2+}]_{cilia}$ rapidly increases, while $[Ca^{2+}]_{cyto}$ near the base of the cilium (circle pos. 2)increases only slightly 40 s later (t = 60 s). Ionomycin added for normalization. Circles in (**c**) indicate areas where fluorescence was measured. (**e**) Distribution of lag times between ciliary and cytoplasmic $[Ca^{2+}]$ increases. (**f**) Calcium diffusion from the cytoplasm to the cilium is not restricted. Red dot indicates the position of calcium uncaging while the white line indicates length and position of line scan. Arrows indicate cytoplasm to cilium transition. Scale bar, 5 μm. See also Supplementary Video 6.

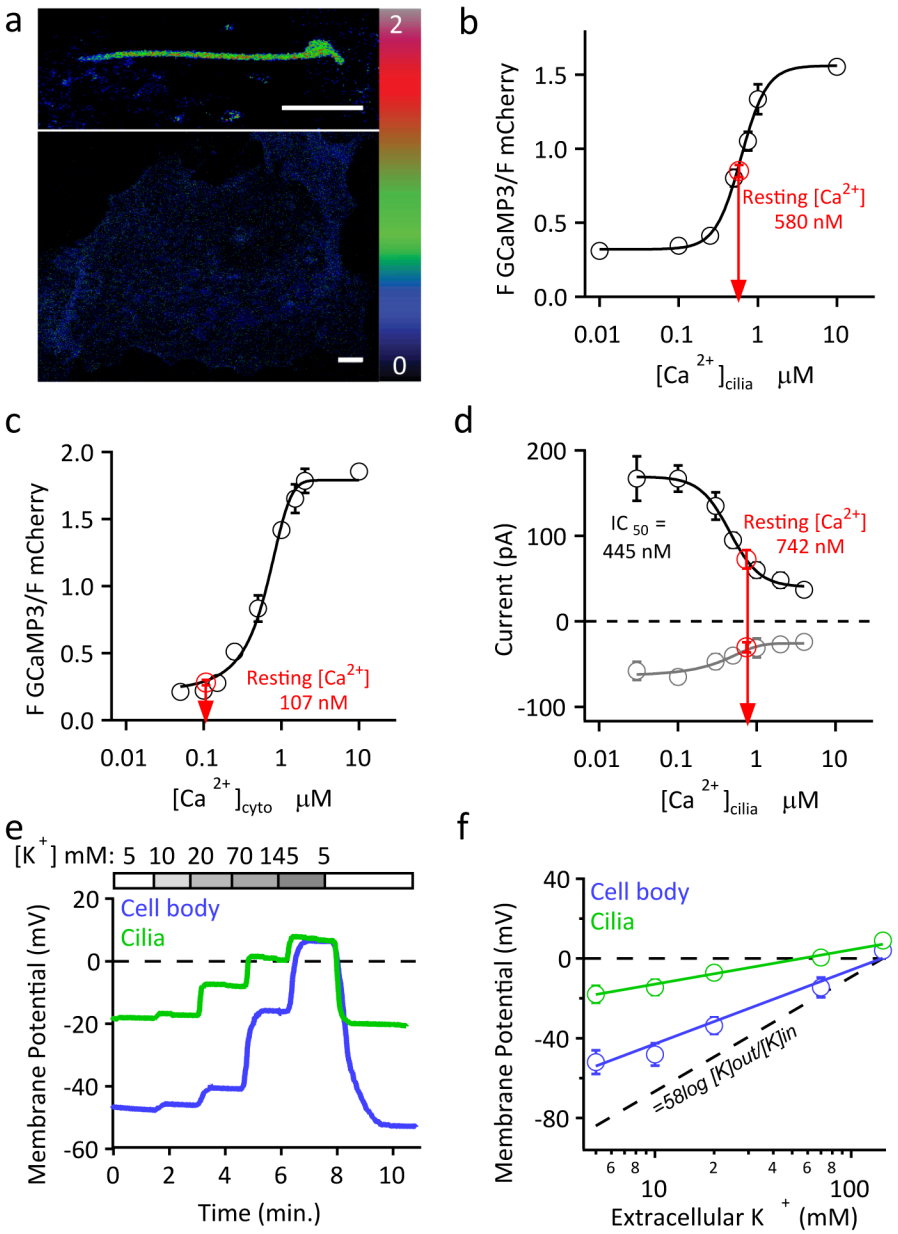

Figure 3. Resting cilium [Ca^{2+}] is substantially higher than resting cytoplasmic [Ca^{2+}]

(**a**) Live hRPE1 cell F GCaMP3/F mCherry ratios in 2mM $[Ca^{2+}]_e$ in the cilium (top) and cytoplasm (bottom). Scale bar, 5 µm. (**b**) Plot of measured ciliary fluorescence ratio (avg. = 0.8 ± 0.12, n = 16 cilia) *vs.* estimated $[Ca^{2+}]_{cilia}$. Resting $[Ca^{2+}]_{cilia}$ = 580 nM. (**c**) Plot of measured cytoplasmic fluorescence ratio (avg. = 0.28 ± 0.02, n = 20 cells) *vs.* estimated $[Ca^{2+}]_{cyto}$. Resting $[Ca^{2+}]_{cyto}$ is 110 nM. (**d**) By measuring current amplitudes in perforated patches (Methods), we estimated resting free $[Ca^{2+}]_{cilia}$ as 742 nM. Black circles = current at +100 mV; grey circles = current at -100 mV. (**e**) Changes in cell (V_m) and cilia (V_{cilia}) potentials in response to external $[K^+]$. (**f**) Average potential of the cell body and cilia plotted as a function of external $[K^+]$. V_m differs from V_{cilia} at all $[K^+]$ other than $[K^+]_e$ = 145mM; $p < 0.05$). The measured resting membrane potential is -18 mV for the cilia and -53

mV for the cell (± SEM, n = 5 cells and 4 cilia). The grey dashed line is the K^+ Nernst potential.

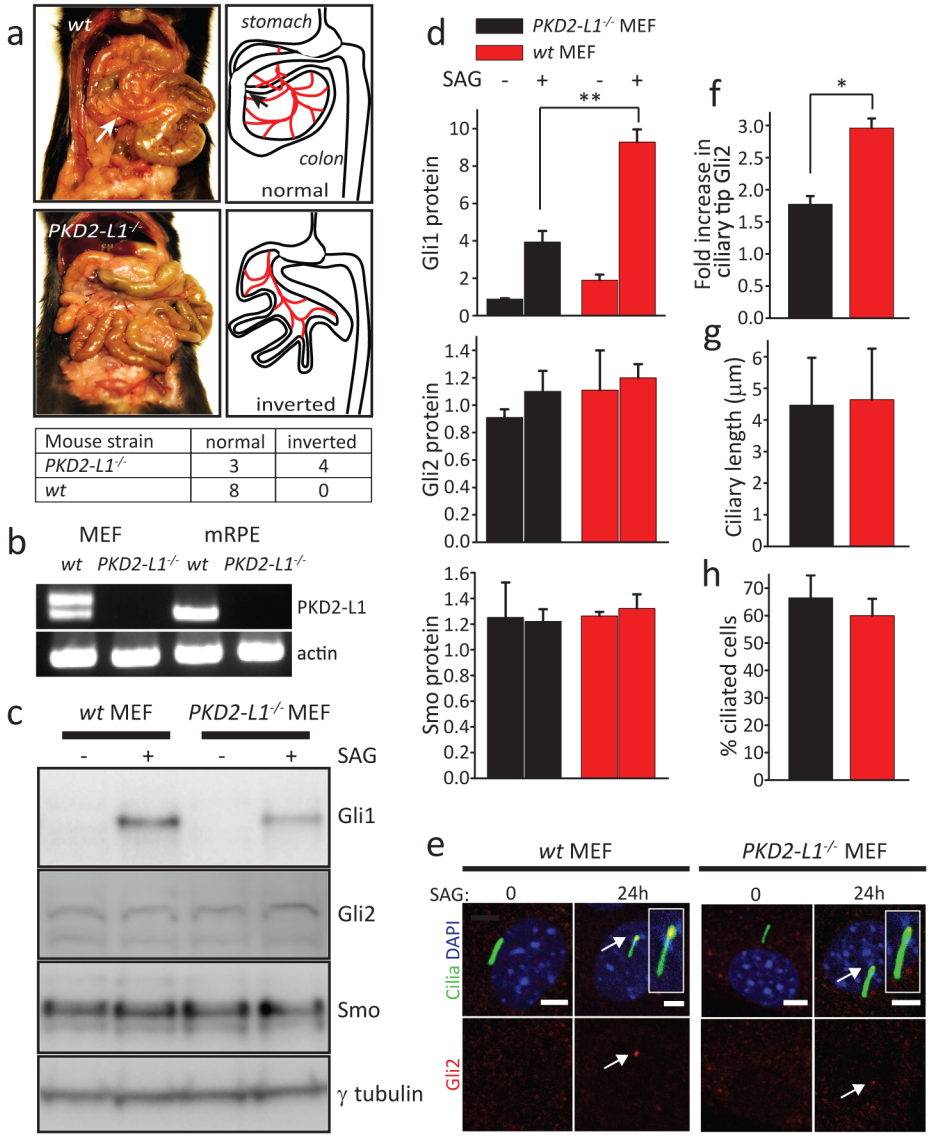

Figure 4. *PKD2-L1*$^{-/-}$ mice exhibit defects in Smo-mediated Gli1 activation

(**a**) Intestinal malrotation in *PKD2-L1*$^{-/-}$ mice, and comparison with *wt*. Arrow indicates correct rotation of intestine. Schematic orientation of intestines is on right, red = mesentery. (**b**) RT-PCR of MEF and mRPE-derived cDNAs shows that PKD2-L1 is expressed in both cell types. (**c**) Western blot of Gli1, Smo, Gli2, and γ-tubulin expression in *wt* and *PKD2-L1*$^{-/-}$ MEFs after stimulation for 24 h with 400 nM SAG. (**d**) *upper panel*: Gli1 in *wt* (1.9 ± 0.3 vs. 9.3 ± 0.7 after stimulation) and *PKD2-L1*$^{-/-}$ MEFs (0.9 ± 0.04 vs. 4.0 ± 0.6 after stimulation). $p < 0.01$. *middle panel*: Gli2 in *wt* (0.9 ± 0.1 vs. 1.1 ± 0.2 after stimulation) vs. *PKD2-L1*$^{-/-}$ MEFs (1.1 ± 0.3 vs. 1.2 ± 0.1 after stimulation). *lower panel*: Smo in *wt* (1.3 ± 0.3 vs. 1.2 ± 0.09 after stimulation) vs. *PKD2-L1*$^{-/-}$ MEFs (1.3 ± 0.04 vs. 1.3 ± 0.1 after stimulation; n = 3 *wt* embryos, 5 *PKD2-L1*$^{-/-}$ embryos). (**e**) Localization of Gli2 at the distal tip of *Arl13B-EGFP*^{tg} and *PKD2-L1*$^{-/-}$ × *Arl13B-EGFP*^{tg} MEF cilia. Scale bar, 5 μm. Arrows point to Gli2 at cilia tips. Cilia are magnified in inserts. (**f**) Quantitation of Gli2

protein accumulation at the ciliary tip after SAG stimulation; *wt*=3.0 ± 0.2 (n=40 cilia each from 3 embryos) vs. *PKD2-L1*$^{-/-}$ MEF = 1.8 ± 0.1 fold increase (n=40 cilia each from 5 embryos). $p < 0.05$. (**g, h**) quantification of ciliary length (4.5 ± 1.5μm for *wt* vs. 4.6 ± 1.6μm for *PKD2-L1*$^{-/-}$ MEFs) and percentage of ciliated cells (67 ± 8% for *wt* vs. 60 ± 6% for *PKD2-L1*$^{-/-}$ MEFs; n=40 cilia each from 3 embryos).